

Quasi-3D Modeling of Li-ion Batteries Based on Single 2D Image

Yoichi Takagishi*, Takumi Yamanaka and Tatsuya Yamaue

Computational Science Center, Kobelco Research Institute Inc., Nishi-ku, Kobe 651-2271, Japan

***Corresponding author**

E-mail Address: takagishi.yoichi@kki.kobelco.com

ORCID

0000-0002-1196-4329

Acknowledgments

Authors' contributions

Y.T designed the study, performed the simulation, and wrote the manuscript; T.Yamanaka and T. Yamaue

designed the study and analyzed the data

Abstract

Electrochemical physics-based simulations of Li-ion batteries using a mesoscale 3D-structure of porous electrodes are one of the most effective approaches for evaluating the local Li concentration in active materials and the Li-ion concentration in electrolytes. However, this approach requires considerable computational resources compared with a simple 2D or 1D homogeneous simulation. In this work, we developed an advanced electrochemical physics-based simulation method for Li-ion batteries that enabled a quasi-3D simulation of charge/discharge using only a single 2D slice image. The governing equations were based on typical theories of electrochemical reactions and ion transport. From referencing the 2D plane, the model was able to simulate both the Li concentration in the active material and the Li-ion concentration in the electrolyte for their subsequent consideration in a virtual 3D structure. To confirm the validity of our proposed model, a full 3D discharge simulation with randomly packed active material particles was performed and compared with the results of the quasi-3D model and a simple-2D model. Results indicated that the quasi-3D model properly reproduced the sliced Li and Li-ion concentrations simulated by the full 3D model in the charge/discharge process, whereas the simple-2D simulation partially overestimated or underestimated these concentrations. In addition, the quasi-3D model made it possible to dramatically decrease the computation time compared to the full-3D model. Finally, we applied the model to an actual Scanning Electron Microscopy equipped with a Focused Ion Beam (FIB-SEM) image of a positive electrode.

Keywords: Li-ion battery, Simulation, Porous structure, SEM

1 Introduction

Lithium-ion (Li-ion) batteries are recognized as the most promising technology for energy storage because of their high energy density, light weight and long cycling life [1, 2]. In addition to various studies on novel materials for electrodes/electrolytes and new battery systems, a variety of simulation technologies [2, 3] have been proposed to predict charge/discharge performances, stress conditions and cycling life times. Electrochemical physics-based models (physicochemical models) [4-25] are useful tools to calculate the various nonlinear resistance components of a battery, including the diffusion of Li, stress in active material particles, electrochemical reactions and ionic transport in electrolytes, while simple equivalent circuit models [26-30] assume that the resistance of the battery is constant or a function of the current and temperature.

Until now, one-dimensional (1D) electrochemical physics-based models, which assume porous electrodes and separators as uniform media, have been widely adopted and developed. These models have been applied to analyze various electrode materials, including $\text{Li}_x\text{Mn}_2\text{O}_4$, LiCoO_2 , LiFePO_4 , and $\text{Li}(\text{NiCoMn})\text{O}_2$, in cathodes and graphite; and Li metal in anodes, along with heat generation, cycle degradation and stress analyses [4-10, 26]. In addition, these models are utilized for systematic studies with a large number of parameter data sets because their calculation costs are relatively low. In the 1D models, however, it is difficult to evaluate nonuniform Li and Li-ion concentrations and reactions, especially in the cross-section of electrodes.

Recently, many studies of charge/discharge simulations based on the mesoscale three-dimensional (3D) structure of porous electrodes have been reported [11-22]. In these cases, porous electrodes were modeled by random packed spheres/hemispheres [11-15] or actual structures based on Scanning Electron Microscopy equipped with a Focused Ion Beam (FIB-SEM) results [17-22] to evaluate the 3D distribution of Li in the active material particles, Li-ion concentration in the electrolyte, and the stress distribution and temperature field of electrodes.

These models enable charge/discharge simulation with realistic 3D electrode structures and provide insightful information at the mesoscale; however, there are some limitations in these models: (1) they require a large-scale amount of calculation and (2) they require 3D tomography data, including 3D-SEM/X-CT results or particle-packed artificial structures, which also require significant cost. Thus, simple two-dimensional (2D) simulations using the cross-sectional structure of a battery electrode have been performed [23-25]. Although these approaches decrease the computational time compared to 3D simulations, they still have some validation problems due to ignoring the effect of the Z-direction.

In this study, we propose a new electrochemical physics-based simulation method for Li-ion batteries that enables a quasi-3D calculation of charge/discharge and a dramatic decrease in the amount of calculation by using a single 2D slice image of porous electrodes for consideration in a virtual 3D structure. In the quasi-3D model, the Li concentration in the active materials and the Li-ion concentration in the electrolyte are simulated in the 2D plane, for consideration in the virtual 3D structure using a single particle model. The study involved the following steps. First, we discuss the inference accuracy of the radius of the active material particle from the 2D plane. Next, the validity and advantage of the calculation cost of this model are confirmed by comparing the results of the 3D discharge simulation with random-packed active material particles. Moreover, we applied the model to an actual FIB-SEM image of a positive electrode and evaluated the distributions of Li and Li-ion concentrations in the plane.

2 Model development

The quasi-3D model is based on electrochemical reaction and ion transport theories, which are widely used in 3D, 2D and 1D models [4-25]. In this model, the Li concentration in the active materials and the Li-ion concentration in the electrolyte are simulated from a 2D slice image of a mesoscale 3D electrode structure in a half-cell. The key idea

of the model is that the Li and Li-ion concentrations are corrected compared to those in the single particle model that is performed in parallel. Here, we introduce the geometric and numerical schemes used in this approach.

2.1 Geometry

In this study, we use a half-cell structure of a positive electrode for galvanostatic discharge simulations. The model geometries for full-3D, simple-2D and quasi-3D simulations are constructed as follows. First, the mesoscale structure of the 3D porous electrode is constructed by randomly packing active material particles. Perfect spheres are assumed to be active material particles and overlaps between these particles are permitted. The radii of the spheres R_{3D} of the spheres are randomly packed sequentially with a uniform distribution in the $L_x \times L_y \times L_z$ simulation cell (the x- and y-axes are the in-plane directions, and the z-axis is the thickness direction of the electrode) until the volume ratio of the active material reaches θ_{AM} . Here, binder and additives are not modeled for the sake of simplicity. Table 1 shows the parameters adopted for generating the 3D porous structure, which are typical values for positive electrodes. This constructed structure is used for a full-3D charge/discharge simulation. Subsequently, slice planes for the simple-2D simulation and quasi-3D simulation are extracted from the middle position of L_y . Fig. 1 illustrates the 3D porous electrode structure and the extracted plane.

2.2 Governing equations of the quasi-3D model

The mathematical model is based on the electrochemistry and Li transport model on the 2D plane for consideration in the virtual 3D structure. The governing equations in the quasi-3D model are listed in Table 2. The Butler-Volmer equation is assumed on the interface between the active particle and electrolyte. The local current density on the interface i_{loc} is described as

$$i_{loc} = i_0 \left[\exp\left(\frac{\alpha F}{RT} \eta\right) - \exp\left(-\frac{\alpha F}{RT} \eta\right) \right] \quad (1)$$

where F , R , α , and i_0 indicate the Faraday constant, gas constant, transfer coefficient, and exchange current density, respectively. Additionally, η denotes the overpotential between the active material and electrolyte

$$\eta = \phi_s - \phi_l - U$$

(2)

where ϕ_s , ϕ_l and U are the active material potential, electrolyte potential and open circuit potential (OCP), respectively. For simplicity, ϕ_s is assumed to be uniform in the active material used in this study. A typical OCP function U for the positive electrode $\text{Li}(\text{NiCoMn})\text{O}_2$ is adopted and written as

$$U = \sum_i p_i (c_s / c_{s,max})^i \quad (3)$$

where $c_{s,max}$ is the coefficient of the maximum Li concentration of the active material, and p_i indicates the coefficient of the polynomial OCV function provided in Table 3.

In the active material particles of an electrode, we assume the modified Fick's law to take into account the effect of the structure in the y-direction. Thus,

$$\frac{\partial c_{s,2D}}{\partial t} = \nabla_{2D} \left[-D_s \nabla_{2D} c_{s,2D}(\mathbf{r}, t) \right] + q_{s,corr} \quad (4)$$

where $c_{s,2D}$ and D_s are the Li concentration in the 2D plane and the Li diffusion coefficient of the active material, respectively. Moreover, $q_{s,corr}$ is used to correct the 2D Li concentration and is described as the difference between the fluxes of Li in the y-axis direction,

$$q_{s,corr} = q_{s,corr}^{surf} + q_{s,corr}^{btm} \quad (5)$$

where $q_{s,corr}^{surf}$ and $q_{s,corr}^{btm}$ are the molar fluxes of the spherical y-axis surface and bottom, respectively. In this

study, we assume that the fluxes are proportional to the concentration gradient, which is evaluated by the reference Li concentrations on the spherical surface $c_{s,surf}^{ref}$ and bottom $c_{s,btm}^{ref}$, and the distances between these positions in the 2D plane (see Fig. 2(a)).

$$q_{s,corr} = \frac{D_s}{d} \left[\frac{c_{s,btm}^{ref}(|\mathbf{r}|, t) - c_{s,2D}(\mathbf{r}, t)}{d_{btm}} - \frac{c_{s,2D}(\mathbf{r}, t) - c_{s,btm}^{ref}(t)}{d_{surf}} \right] \quad (6)$$

where the d parameters are determined by the geometric structure of the electrode. In this study, the average length between the surface and bottom of the sphere, $d=0.5R_{3D}$, is adopted. The reference Li concentrations $c_{s,surf}^{ref}$ and $c_{s,btm}^{ref}$ are estimated by a single-particle model that is conducted in parallel.

The Li-ion concentration $c_{l,2D}$ and potential $\phi_{l,2D}$ in the electrolyte are estimated by the mass conservation law and Nernst-Planck equation,

$$\frac{\partial c_{l,2D}}{\partial t} = \nabla_{2D}[-D_l \nabla_{2D} c_{l,2D}(\mathbf{r}, t)] + q_{l,corr} \quad (7)$$

$$\nabla_{2D} \cdot \left(-\sigma_l \nabla_{2D} \phi_{l,2D} + \frac{2\sigma_l RT}{F} (1 - t_+) \nabla \ln c_{l,2D} \right) = 0 \quad (8)$$

where D_l , σ_l and t_+ are the diffusion coefficient, ionic conductivity and transport number in the electrolyte, respectively. At the boundary between the electrode and separator ($z=0 \mu\text{m}$), the Dirichlet condition $c_l^{ref} = c_{l,0}$ is applied. The 2nd term of the right-hand side of Eq. (7) $q_{l,corr}$ is a source term to correct the 2D Li-ion concentration with the reference Li-ion concentration c_l^{ref} ,

$$q_{l,corr} = \frac{D_l}{d_l} \left[2 \frac{c_l^{ref}(\mathbf{r}, t) - c_{l,2D}(t)}{d_l} \right] \quad (9)$$

where d_l is the parameter for the distance to the reference concentration. Herein, we assume d_l to be $10 \mu\text{m}$, which is the representative length in the electrolyte. Fig. 2(b) shows a schematic image of the correction of the 2D Li-ion concentration.

As mentioned above, the reference Li and Li-ion concentrations are estimated by the single-particle model conducted in parallel. The reference Li concentration in the active material c_s^{ref} is written as the 1D diffusion equation,

$$\frac{\partial c_s^{ref}}{\partial t} = D_s \frac{1}{r^2} \frac{\partial}{\partial r} \left[r^2 \frac{\partial c_s^{ref}}{\partial r} \right] \quad (10)$$

with the Neumann boundary condition

$$D_s \frac{\partial c_s^{ref}}{\partial r} \Big|_{r=R} = j_{ave} = \frac{i_{app}}{F \theta_{AM} L_z} \quad (11)$$

where j_{ave} means the average molar flux associated with the electrochemical reaction between the active material and electrolyte and i_{app} indicates the applied current density. On the other hand, the reference Li-ion concentration in the electrolyte is evaluated by

$$c_l^{ref} = c_{l,0} - \frac{L_z}{2D_l} \frac{j_{ave}}{(1 - \theta_{AM})} \quad (12)$$

Thus, we ignore the relaxation time of the Li-ion concentration in the electrolyte in this description. The parameters for the typical positive electrode Li(NiCoMn)O₂ [**] and electrolyte 1 M LiPF₆/EC:DEC=1:1 by volume are adopted and listed in Table 4.

2.3 Estimation of R_{3D} from the 2D plane

In the quasi-3D model, the actual radius of the 3D active material R_{3D} is required to calculate the reference Li concentration c_s^{ref} . However, R_{3D} is not equal to R_{2D} because the “active material disc” on the 2D plane is a result of a randomly sliced “active material sphere”. Herein, we use a Bayesian inference to determine R_{3D} from the 2D

plane.

$$P(\theta|x) \propto P(\theta)P(x|\theta) \quad (13)$$

where $P(\theta|x)$, $P(\theta)$, and $P(x|\theta)$ indicate the posterior distribution, prior distribution, and likelihood, respectively. The probability of the radius of the active material on the 2D plane (disc shape), R_{2D} , from the actual radius R_{3D} in 3D (spherical shape) is described as

$$P(R_{2D}|R_{3D}) = \frac{\sqrt{R_{3D}^2 - (R_{3D} - R_{2D})^2}}{R_{3D}} \quad (14)$$

Assuming that we have no prior information about R_{3D} , the prior can be described as

$$P(R_{3D}) = \text{const.} \quad (15)$$

according to the principle of insufficient reason. Therefore, the posterior of R_{2D} on the 2D plane from the R_{3D} of the active material sphere can be written as

$$P(R_{3D}|R_{2D}) \propto \prod_i \frac{\sqrt{R_{3D}^2 - (R_{3D} - R_{2D,i})^2}}{R_{3D}} \quad (16)$$

where $R_{2D,i}$ indicates the i th radius of the active material disc on the 2D plane.

2.4 Governing equations of the full-3D and simple-2D models

The governing equations in the full-3D and simple-2D models are based on electrochemistry and Li transport theories without the correction introduced in the quasi-3D mode. The mass conservation equation of the Li concentration is applied to the active material, and the Nernst-Planck equation and mass conservation equation are adopted to evaluate the potential and Li-ion concentration in the electrolyte. The Butler-Volmer equation is used on the interface between the active particle and electrolyte. In addition to the quasi-3D model, the potential in the active material is assumed to be uniform for simplicity. The governing equations in the full-3D and simple-2D models are

listed in Table 5.

The modeling and calculation of the three models were performed using COMSOL Multiphysics™ ver. 5.4 with a standard workstation containing a 16-core Intel Xeon™ (2.60 GHz) processor and 128 GB of RAM.

3 Results and discussion

The proposed quasi-3D model was validated with a full-3D model and compared to a simple-2D model under various applied current densities. First, the 3D active material radius R_{3D} was estimated from the radius of the active material disc R_{2D} by a Bayesian inference. Additionally, we carried out galvanostatic discharge simulations at a low current density and evaluated their results, including the Li concentration in the active material, Li-ion concentration in the electrolyte, and voltage profile. Finally, simulations at a high current density were conducted, and the model limitations and robustness were discussed.

3.1 Estimation of R_{3D}

The center positions and radius of each active material disc in the 2D slice structure, shown in Fig. 1(b), were detected by the watershed method. The histograms of the detected radii of 16 active material discs are shown in Fig. 3(a). Most radii are near 10-11 μm . Using these radii, we estimated the 3D active material radius R_{3D} by a Bayesian inference as described in Eq. (16). Fig. 3(b) shows the posterior distribution of R_{3D} . Note that the vertical axis is described as an arbitrary unit. The highest probability is located at approximately 10.5 μm , which is close to the actual radius of 11.0 μm . This indicates that the actual 3D radius of the active material sphere can be inferred from the 2D radii of the discs on an arbitrarily sliced image. Although a large number of discs improves the estimation accuracy, the slice image that includes only 16 discs used in this study is sufficient to infer the actual 3D radius. The

difference in accuracy of the R_{3D} inference using the slice position has been discussed in the Appendix.

3.2 Low current density (0.5C)

Galvanostatic discharge simulations at 0.5C (4.81 [A/m²]) were conducted using the full-3D, quasi-3D and simple-2D models. The cell voltage profiles in these models are described in Fig. 4. The discharge voltages within 7000 s in the 2D-simple and quasi-3D models are close to those in the full-3D model. However, the simple-2D model overestimates the capacity (the voltage drops at approximately 9000 s), whereas the quasi-3D model estimates it more accurately than the full-3D model (the voltage drops at approximately 7200 s). Fig. 5 shows the Li concentration in the active material at 50% SOC. In the 3D view of the full-3D model (Fig. 5(a)), one can see the concentration gradient from the surface to the center of the sphere. We compared the slice image of the full-3D concentration with that of the quasi-3D and simple-2D concentrations, as shown in Fig. 5(b). The simple-2D model underestimates the Li concentration inside the large region (point A) and overestimates it in the small region (point B) because it simulates only the 2D plane (x-z plane), ignoring the flux in the y-direction. On the other hand, the Li concentration in the active material of the quasi-3D model agrees well with the full-3D mode because of the correction with the average concentration of the single-particle model. Fig. 6(a) illustrates the concentration profiles of these models on the X_1 - X_1' lines. It is apparent that the profile of the quasi-3D model is close to that of the full-3D model, whereas the predicted concentration of the simple-2D model is relatively poor. The time sequence of Li concentrations at points A and B in these models is described in Fig. 6(b) and (c), respectively. Compared with the poor agreement of the simple-2D model at both points, the Li concentration and its increase in the quasi-3D model agree with those in the full-3D model.

The Li-ion concentration in the electrolyte at 50% SOC is illustrated in Fig. 7. As seen in Fig. 7(a), the

concentration gradient is formed from the boundary of the separator (bottom plane) to the boundary of the current collector (top plane). The slice image of the full-3D concentration is compared with that of the quasi-3D and simple-2D concentrations, as shown in Fig. 7(b). The simple-2D model underestimates the Li-ion concentration over the whole electrolyte region because it ignores the flux in the y-direction. The Li-ion concentrations on the X_2 - X_2' lines are illustrated in Fig. 8(a). Compared to that of the simple-2D model, the concentration profile of the quasi-3D model is relatively close to that of the full-3D model. In Fig. 8(b), the variation of the Li-ion concentrations over time at point C of these models is described. Additionally, compared to those in the simple-2D model at both points, the Li-ion concentration and its increase in the quasi-3D model are relatively close to those in the full-3D model at both points.

3.3 High current density (1C and 2C)

Discharge simulations of the full-3D, simple 2D and quasi-3D models were carried out at high current densities of 1C and 2C. A comparison of the discharge curves of the three models is described in Fig. 9. At 1C, the voltages within 2800 s in the simple-2D and quasi-3D models are close to that in the full-3D model. The simple-2D model apparently overestimates the capacity (the voltage drops at approximately 3700 s), whereas the quasi-3D model estimates it more accurately and matches more closely to the full-3D model (the voltage drops at approximately 3100 s). On the other hand, the discharge voltage of the simple-2D model at 2C drops rapidly at the beginning of the simulation due to Li-ion exhaustion near the active material in the electrolyte. Notably, the voltages of the quasi-3D and full-3D models are similar to each other at 0.5C and 1C.

The Li concentrations in the active material at 50% SOC of the models are shown in Fig. 10. Note that the data of 2C in the simple-2D model is not available because of a calculation failure. As evidenced in the 0.5C case,

the simple-2D model underestimates the Li concentration inside the large region (point A) and overestimates it in the small region (point B), whereas those in the active material of the quasi-3D model agree well with the full-3D model.

To evaluate the prediction accuracy of the models, the derivation between the simulated values of the full-3D model and those of the quasi-3D/simple-2D models is defined as follows:

$$Error = \sum_i x_{i,F3D} - x_{i,m} \quad (17)$$

where $x_{i,F3D}$ and $x_{i,m}$ indicate the simulated value of the full-3D model and the quasi-3D/simple-2D models

(m=Q3D, S2D). Fig. 11(a) shows the derivation of the Li concentration in the active material at 0.5, 1.0 and 2.0C.

Not that there are no data of the simple-2D model at the 2C discharge condition due to the rapid voltage drop at the beginning of the simulation. It is apparent that the derivations of both models increase with the C-rate because the large molar flux at the boundary between the active material and electrolyte leads to the nonuniform concentration in the active material having a larger effect. At 1C, the derivation of the quasi-3D model (595 mol/m³) remains lower than the value of the simple-2D model (1518 mol/m³). The same tendency is seen in the Li-ion concentration in the electrolyte, as described in Fig. 11(b). The derivations of both models increase with the C-rate, whereas at 1C the derivation of the quasi-3D model (155 mol/m³) remains lower than the value of the simple-2D model (295 mol/m³).

These results indicate that the quasi-3D model can be a useful tool to predict the Li and Li-ion concentrations in the 2D plane as long as the applied C-rate is not relatively large.

3.4 Computation time

Table 6 shows a comparison of the calculation times of the full-3D and quasi-3D models at 0.5C. The calculation

time of the quasi-3D model is approximately one hundred times that of the full-3D model. Thus, the quasi-3D model using a single slice image makes it possible to dramatically decrease the calculation cost while still providing accurate cell voltages and Li and Li-ion concentration distributions.

4 Application to an actual FIB-SEM image

The proposed quasi-3D modeling is expected to be applied to an actual electrode structure. To test the model with an actual electrode structure, a discharge simulation using an FIB-SEM image of a positive electrode $\text{Li}(\text{NiCoMn})_{1/3}\text{O}_2$ was conducted. In addition to the scheme for the particle packing structure described previously, the 3D active material radius R_{3D} was estimated from the active material radius R_{2D} obtained from an SEM image by a Bayesian inference. Subsequently, we carried out galvanostatic discharge simulations at 1C with typical parameters.

4.1 FIB-SEM image segmentation and inference of the active material size

Herein, the FIB-SEM image positive electrode $\text{Li}(\text{NiCoMn})_{1/3}\text{O}_2$, which was taken in a previous study [31], was used, and image segmentation was conducted to produce two regions (active material and electrolyte). Fig. 12 shows the FIB-SEM image and segmentalized image. Subsequently, we detected the radius of each active material on the 2D slice structure. As shown in Fig. 12(a), the active material particles are not spherical but polyhedral, and R_{2D} is evaluated using their circumscribed circles. A histogram of the radii of 111 active material polygons is shown in Fig. 13(a). Using these radii, we estimate the 3D active material radius R_{3D} by a Bayesian inference as described in Eq. (16). Fig. 13(b) describes the posterior distribution of R_{3D} . The highest probability is located at approximately 12 μm . It should be noted that this inference is based on the hypothesis that all active material particles are the same size, whereas the actual size distribution has multiple peaks (2-3 and 7 μm). Therefore, the inferred R_{3D} is not

necessarily accurate and is a future challenge.

4.2 Galvanostatic simulation based on the FIB-SEM image

Galvanostatic discharge simulations at 2C ($19.2 \text{ [A/m}^2\text{]}$) were conducted using the segmented FIB-SEM image.

Although the parameters for the simulation should be determined in each system, we adopted the same parameters used in the spherical packing structure (Table 4) to test the application possibility of the quasi-3D model to an actual structure. Fig. 14 describes the Li and Li-ion concentration distributions at $t=1000 \text{ s}$. In regard to the Li concentration in the active material, the concentration gradient is confirmed from the surface to the center of the active material polygons. On the other hand, the Li-ion concentration in the electrolyte is relatively high near the narrow regions. These results indicate that the quasi-3D model can be applicable to segmented FIB-SEM images with properly determined parameter values.

5 Conclusion

In this study, we proposed a new electrochemical physics-based simulation method for Li-ion batteries that enables a quasi-3D calculation of charge/discharge and a dramatic decrease in the amount of calculation by using a single 2D slice image of porous electrodes for consideration in a virtual 3D structure.

First, the actual 3D radius of the active material sphere was inferred from the 2D radii of discs on an arbitrarily sliced image. Although a larger number of discs improves the estimation accuracy, we concluded that the slice image including only 16 discs used in this study was sufficient to infer the actual 3D radius. Subsequently, the quasi-3D model was validated with the full-3D model and compared to the results of the simple-2D model at 0.5, 1.0 and 2.0C. As a result, the evaluated Li concentration in the active material, Li-ion concentration in the

electrolyte, and voltage profile by the quasi-3D model were close to those of the full-3D model, whereas those of the simple-2D model were relatively poor. Finally, we compared the calculation costs of these models and confirmed that the quasi-3D model using a single slice image made it possible to dramatically decrease the calculation cost.

Appendix

To confirm the difference in the accuracy of the R_{3D} inference due to the slice position of the actual 3D structure, we compare the estimated R_{3D} from the slice positions $y=1/3L_y$, $2/3L_y$ and $3/3L_y$ (see Fig. 15(a)) in addition to the case of $y=1/2L_y$, described in Section 3.1. The number of active material discs on the plane is 15 in the case of $y=1/3L_y$, 9 in the case of $y=2/3L_y$, and 16 in the case of $y=3/3L_y$. Fig. A1(b) shows the histogram of detected radii in these three cases. Most radii are near 10.5-12.0 μm in all cases. Using these radii, we estimate the 3D active material radius R_{3D} by a Bayesian inference as described in Eq. (16). Fig. A1(c) describes the posterior distribution of R_{3D} . Although there are some fluctuations between them, the highest probability of R_{3D} is located at approximately 10-11 μm . Thus, we can conclude that the accuracy of the R_{3D} inference at various slice positions is almost the same in this structure. However, note that the accuracy may change based on the system size, number of particles and particle size. Namely, the larger the system size is, the larger the number of particles; thus, the inference accuracy increases.

Declarations

Funding

Conflicts of interest/Competing interests

The authors have no conflicts of interest to declare that are relevant to the content of this article.

Availability of data and material

Code availability

Reference

1. Etacheri V, Marom R, Elazari R, Salitra G, Aurbach D (2011) Challenges in the development of advanced Li-ion batteries: a review. *Energy Environ Sci* 4:3243-3262. <https://doi.org/10.1039/c1ee01598b>
2. Lu L, Han X, Li J, Hua J, Ouyang M (2013) A review on the key issues for Lithium-ion battery management in electric vehicles. *J Power Sources* 226:272-288. <https://doi.org/10.1016/j.jpowsour.2012.10.060>
3. Ramadesigan V, Northrop PW, De S, Santhanagopalan S, Braatz RD, Subramanian VR (2012) Modeling and simulation of lithium-ion batteries from a systems engineering perspective. *J Electrochem Soc* 159:R31-R45. <https://doi.org/10.1149/2.018203jes>
4. Doyle M, Newman J, Gozdz AS, Schmutz CN, Tarascon JM (1996) Comparison of modeling predictions with experimental data from plastic lithium ion cells. *J Electrochem Soc* 143:1890-1903. <https://doi.org/10.1149/1.1836921>
5. Fang W, Kwon OJ, Wang CY (2010) Electrochemical-thermal modeling of automotive Li-ion batteries and experimental validation using a three-electrode cell. *Int J Energy Res* 34:107-115. <https://doi.org/10.1002/er.1652>
6. Ning G, Popov BN (2004) Cycle life modeling of Lithium-ion batteries. *J Electrochem Soc* 151:A1584-A1591. <https://doi.org/10.1149/1.1787631>
7. Ramadass P, Haran B, Gomadam PM, White R, Popov BN (2004) Development of first principles capacity fade model for Li-ion cells. *J Electrochem Soc* 151:A196-A203. <https://doi.org/10.1149/1.1634273>
8. Takagishi Y, Yamaue T (2017) Prediction of Li-ion battery module performance under running condition based on “Multifactorial degradation model”. *Int J Automot Eng* 8:137-142.

- https://doi.org/10.20485/jsacijae.8.3_143
9. Hosseinzadeh E, Marco J, Jennings P (2017) Electrochemical-thermal modelling and optimisation of Lithium-ion battery design parameters using analysis of variance. *Energies* 10:1278.
<https://doi.org/10.3390/en10091278>
 10. Wu W, Xiao X, Huang X (2012) The effect of battery design parameters on heat generation and utilization in a Li-ion cell. *Electrochim Acta* 83:227-240. <https://doi.org/10.1016/j.electacta.2012.07.081>
 11. Latz A, Zausch J (2015) Multiscale modeling of Lithium-ion batteries: thermal aspects. *Beilstein J Nanotechnol* 6:987-1007. <https://doi.org/10.3762/bjnano.6.102>
 12. Feinauer J, Hein S, Rave S, Schmidt S, Westhoff D, Zausch J, Iliev O, Latz A, Ohlberger M, Schmidt V (2019) MULTIBAT: unified workflow for fast electrochemical 3D simulations of Lithium-ion cells combining virtual stochastic microstructures, electrochemical degradation models and model order reduction. *J Comput Sci* 31:172-184. <https://doi.org/10.1016/j.jocs.2018.03.006>
 13. Bertei A, Nucci B, Nicoletta C (2013) Effective transport properties in random packings of spheres and agglomerates. *Chem Eng Trans* 32:1531-1536
 14. Trembacki B, Duoss E, Oxberry G, Stadermann M, Murthy J (2019) Mesoscale electrochemical performance simulation of 3D interpenetrating Lithium-ion battery electrodes. *J Electrochem Soc* 166:A923-A934. <https://doi.org/10.1149/2.0031906jes>
 15. Rucci A, Ngandjong AC, Primo EN, Maiza M, Franco AA (2019) Tracking variabilities in the simulation of Lithium-ion battery electrode fabrication and its impact on electrochemical performance. *Electrochim Acta* 312:168-178. <https://doi.org/10.1016/j.electacta.2019.04.110>
 16. Takagishi Y, Yamanaka T, Yamaue T (2019) Machine learning approaches for designing mesoscale

- structure of Li-ion battery electrodes. *Batteries* 5:54. <https://doi.org/10.3390/batteries5030054>
17. Less GB, Seo JH, Han S, Sastry AM, Zausch J, Latz A, Schmidt S, Wieser C, Kehrwald D, Fell S (2012) Micro-scale modeling of Li-ion batteries: parameterization and validation. *J Electrochem Soc* 159:A697-A704. <https://doi.org/10.1149/2.096205jes>
 18. Lu X, Bertei A, Finegan DP, Tan C, Daemi SR, Weaving JS, O'Regan KB, Heenan TMM, Hinds G, Kendrick E, Brett DJL, Shearing PR (2020) 3D microstructure design of Lithium-ion battery electrodes assisted by X-ray nano-computed tomography and modelling. *Nat Commun* 11:2079. <https://doi.org/10.1038/s41467-020-15811-x>
 19. Kashkooli AG, Amirfazli A, Farhad S, Lee DU, Felicelli S, Park HW, Feng K, De Andrade V, Chen Z (2017) Representative volume element model of Lithium-ion battery electrodes based on X-ray nanotomography. *J Appl Electrochem* 47:281-293. <https://doi.org/10.1007/s10800-016-1037-y>
 20. Trembacki BL, Mistry AN, Noble DR, Ferraro ME, Mukherjee PP, Roberts SA (2018) Mesoscale analysis of conductive binder domain morphology in Lithium-ion battery electrodes. *J Electrochem Soc* 165:E725-E736. <https://doi.org/10.1149/2.0981813jes>
 21. Gelb J, Finegan D, Brett D, Shearing P
 22. Lagadec MF, Zahn R, Wood V (2018) Designing polyolefin separators to minimize the impact of local compressive stresses on Lithium-ion battery performance. *J Electrochem Soc* 165:A1829-A1836. <https://doi.org/10.1149/2.0041809jes>
 23. Meyer M, Komsijska L, Lenz B, Agert C (2013) Study of the local SOC distribution in a Lithium-ion battery by physical and electrochemical modeling and simulation. *Appl Math Model* 37:2016-2027. <https://doi.org/10.1016/j.apm.2012.04.029>

24. Wu W, Xiao X, Wang M, Huang X (2014) A microstructural resolved model for the stress analysis of Lithium-ion batteries. *J Electrochem Soc* 161:A803-A813. <https://doi.org/10.1149/2.082405jes>
25. Bucci G, Swamy T, Bishop S, Sheldon BW, Chiang YM, Carter WC (2017) The effect of stress on battery-electrode capacity. *J Electrochem Soc* 164:A645-A654. <https://doi.org/10.1149/2.0371704jes>
26. Krewer U, Röder F, Harinath E, Braatz RD, Bedürftig B, Findeisen R (2018) Dynamic models of Li-ion batteries for diagnosis and operation: a review and perspective. *J Electrochem Soc* 165:A3656-A3673. <https://doi.org/10.1149/2.1061814jes>
27. Dong T, Kirchev A, Mattera F, Kowal J, Bultel Y (2011) Dynamic modeling of Li-ion batteries using an equivalent electrical circuit. *J Electrochem Soc* 158:A326-A336. <https://doi.org/10.1149/1.3543710>
28. Lee J, Lee J, Nam O, Kim J, Cho BH, Yun H, Choi S, Kim K, Kim JH, Jun S (2006) Modeling and real time estimation of lumped equivalent circuit model of a Lithium-ion battery. In: 12th international power electronics and motion control conference, IEEE, Portoroz, Slovenia, pp 1536-1540
29. Madani SS, Schaltz E, Knudsen Kær S (2019) An electrical equivalent circuit model of a lithium titanate oxide battery. *Batteries* 5:31. <https://doi.org/10.3390/batteries5010031>
30. Liaw BY, Nagasubramanian G, Jungst RG, Doughty DH (2004) Modeling of Lithium-ion cells—A simple equivalent-circuit model approach. *Solid State Ion* 175:835-839. <https://doi.org/10.1016/j.ssi.2004.09.049>
31. Tsubota T, Achiha T, Hayashi Y, Syu R, Ikeda T, Nishiuchi M (2016) Kobelco technology review no.34, p. 65. Secretariat & Publicity Dept. Kobe Steel, Ltd., Hyogo, Japan

Tables

Table 1. Parameters for generating the 3D porous structure.

Parameter	Value
Active material particle radius, R_{3D}	11.0 [μm]
Simulation cell size, L_x (in-plane direction)	100 [μm]
L_y (in-plane direction)	100 [μm]
L_z (thickness direction)	50 [μm]
Volume ratio of active material, θ_{AM}	0.58
Overlap distance, d_{ov}	$0 < d_{ov} < 1$ [μm]

Table 2. Governing equations in the quasi-3D model.

	2D-plane simulation	Correction term	Reference concentration
Li concentration in the active material	$\frac{\partial c_{s,2D}}{\partial t} = \nabla_{2D}[-D_s \nabla_{2D} c_{s,2D}] + q_{s,corr}$	$\frac{D_s}{d} \left[\frac{c_{s,btm}^{ref} - c_{s,2D}}{d_{btm}} - \frac{c_{s,2D} - c_{s,btm}^{ref}}{d_{surf}} \right]$	$\frac{\partial c_s^{ref}}{\partial t} = D_s \frac{1}{r^2} \frac{\partial}{\partial r} \left[r^2 \frac{\partial c_s^{ref}}{\partial r} \right]$
Li-ion concentration in the electrolyte	$\frac{\partial c_{l,2D}}{\partial t} = \nabla_{2D}[-D_l \nabla_{2D} c_{l,2D}] + q_{l,corr}$	$\frac{D_l}{d_l} \left[2 \frac{c_l^{ref} - c_{l,2D}}{d_l} \right]$	$c_l^{ref} = c_{l,0} - \frac{L_z}{2D_l} \frac{j_{ave}}{(1 - \theta_{AM})}$
Potential in the electrolyte	$\nabla_{2D} \cdot \left(-\sigma_l \nabla_{2D} \phi_{l,2D} + \frac{2\sigma_l RT}{F} (1 - t_+) \nabla \ln c_{l,2D} \right) = 0$	—	—
Electrochemical reaction at the interface	$i_{loc} = i_0 \left[\exp\left(\frac{\alpha F}{RT} \eta\right) - \exp\left(-\frac{\alpha F}{RT} \eta\right) \right]$	—	$j_{ave} = \frac{i_{app}}{F \theta_{AM} L}$

Table 3. Coefficients of the polynomial open circuit voltage (OCV) function [8].

Coefficient	Value
p_6	-611.13
p_5	2375.3
p_4	-3797.4
p_3	3196.0
p_2	-1491.8
p_1	364.33
p_0	-31.858

Table 4. Parameters for the charge/discharge simulations.

Parameters	Value	Reference
Diffusion coefficient in the active material, D_s	1.0×10^{-14} [m ² /s]	Assumed
Diffusion coefficient in the electrolyte, D_l	1.0×10^{-11} [m ² /s]	Assumed
Ionic conductivity in the electrolyte, σ_l	0.1 [S/m]	Assumed
Transfer number, t_+	0.363	[14]
Exchange current density, i_0	0.5 [A/m ²]	Assumed
Transfer coefficient, α	0.5	[14]
Temperature, T	298 [K]	Assumed
Applied current density, i_{app}	4.81 (0.5C), 9.62 (1C), 19.2 (2C) [A/m ²]	-
Maximum Li concentration in the active material, $c_{s,max}$	31000 [mol/m ³]	[23]

Table 5. Governing equations in the full-3D and simple-2D models.

	Equation
Li concentration in the active material	$\frac{\partial c_s}{\partial t} = \nabla_n[-D_s \nabla_n c_s]$
Li-ion concentration in the electrolyte	$\frac{\partial c_l}{\partial t} = \nabla_n[-D_l \nabla_n c_l]$
Potential in the electrolyte	$\nabla_n \cdot \left(-\sigma_l \nabla_n \phi_l + \frac{2\sigma_l RT}{F} (1 - t_+) \nabla \ln c_l \right) = 0$
Electrochemical reaction at the interface	$i_{loc} = i_0 \left[\exp\left(\frac{\alpha F}{RT} \eta\right) - \exp\left(-\frac{\alpha F}{RT} \eta\right) \right]$

Table 6. Comparison of computation time among the full-3D, quasi-3D, and simple-2D models at 0.5C.

Model	Computation time [min]
<i>Full-3D</i>	210
<i>Quasi-3D</i>	2.3
<i>Simple-2D</i>	2.2

Figure captions

Fig. 1 Geometries used in this study for (a) the full-3D porous electrode structure and (b) extracted plane

Fig. 2 Schematic image showing the correction of the (a) 2D Li-ion concentration in the active material and the (b) 2D Li-ion concentration in the electrolyte

Fig. 3 (a) Histogram of the detected radii of 16 active materials on a 2D slice image (b) Posterior distribution of R_{3D}

Fig. 4 Simulated cell voltage profiles of the full-3D, quasi-3D and simple-2D models at 0.5C

Fig. 5 Li concentration in the active material at 50% SOC at a low current density (0.5C). (a) The 3D view of the full-3D model. (b) Slice image of the full-3D, simple-2D and quasi-3D models

Fig. 6 (a) Concentration profiles of these models on the X_1 - X_1' lines, and the (b) time sequence of the Li concentrations at point A and (c) point B

Fig. 7 Li-ion concentration in the electrolyte at 50% SOC at a low current density (0.5C). (a) The 3D view of the full-3D model. (b) Slice image of the full-3D, simple-2D and quasi-3D models

Fig. 8 (a) Li-ion concentration profiles of these models on the X_2 - X_2' lines, and the (b) time sequence of the Li concentrations at point C

Fig. 9 Comparison of the discharge curves of the full-3D, quasi-3D, and simple-2D models at (a) 1.0C and (b) 2.0C

Fig. 10 Li concentrations in the active material at 50% SOC for all three models

Fig. 11 Derivation of the simulated values between the quasi-3D/simple-2D models and the full-3D model at 0.5, 1.0 and 2.0C. (a) Li concentration in the active material, and the (b) Li-ion concentration in the electrolyte

Fig. 12 (a) FIB-SEM image of the positive electrode [31] (b) Segmented FIB-SEM image. The white and black regions indicate the active material and electrolyte, respectively

Fig. 13 (a) Histogram of the radii for 111 active material polygons (b) The posterior distribution of R_{3D}

Fig. 14 Concentration distribution at 1C for 1000 s. (a) Li concentration in the active material, and the (b) Li-ion concentration in the electrolyte

Fig. A1 (a) Estimated R_{3D} from the slice position $y= 1/3L_y, 2/3L_y$ and $3/3L_y$, (b) histogram of the detected radii in these three cases, and (c) posterior distribution of R_{3D}

Figures

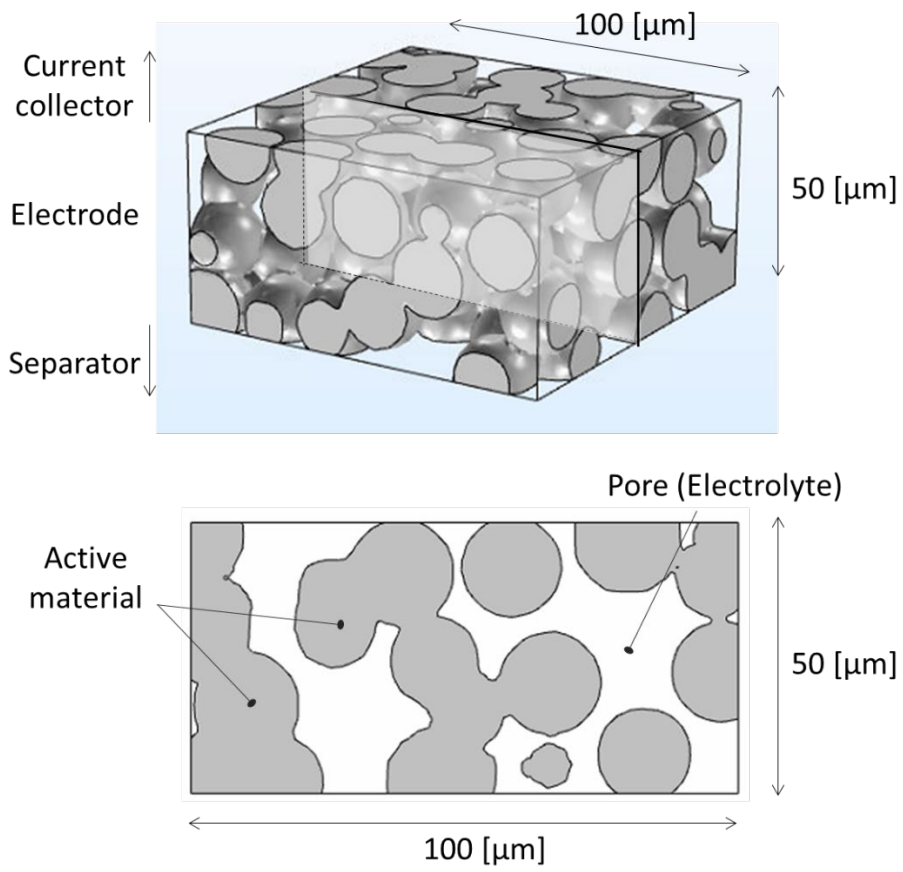
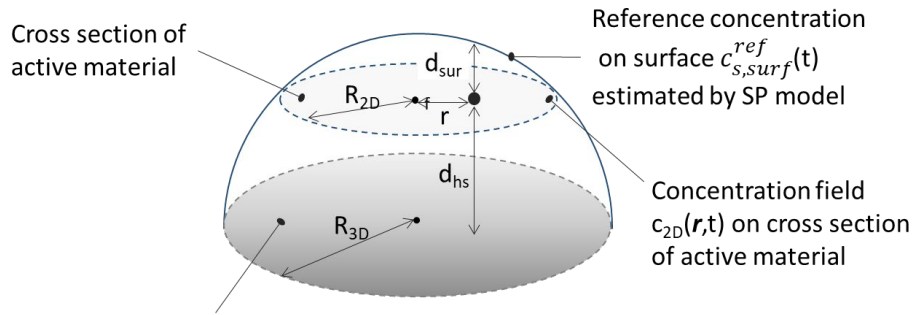


Fig. 1

(a)



Reference concentration field $c_{s,btm}^{ref}$ on hemisphere bottom estimated by SP model

(b)

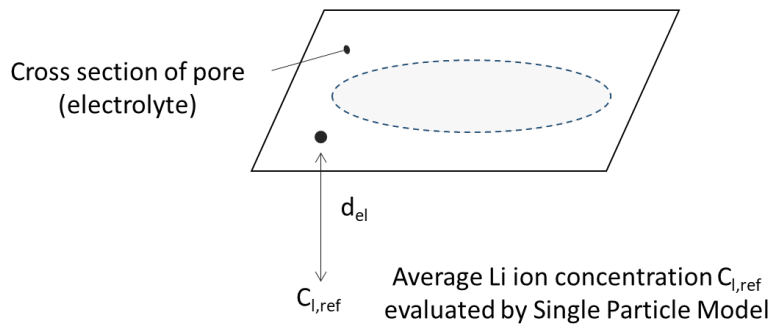


Fig. 2

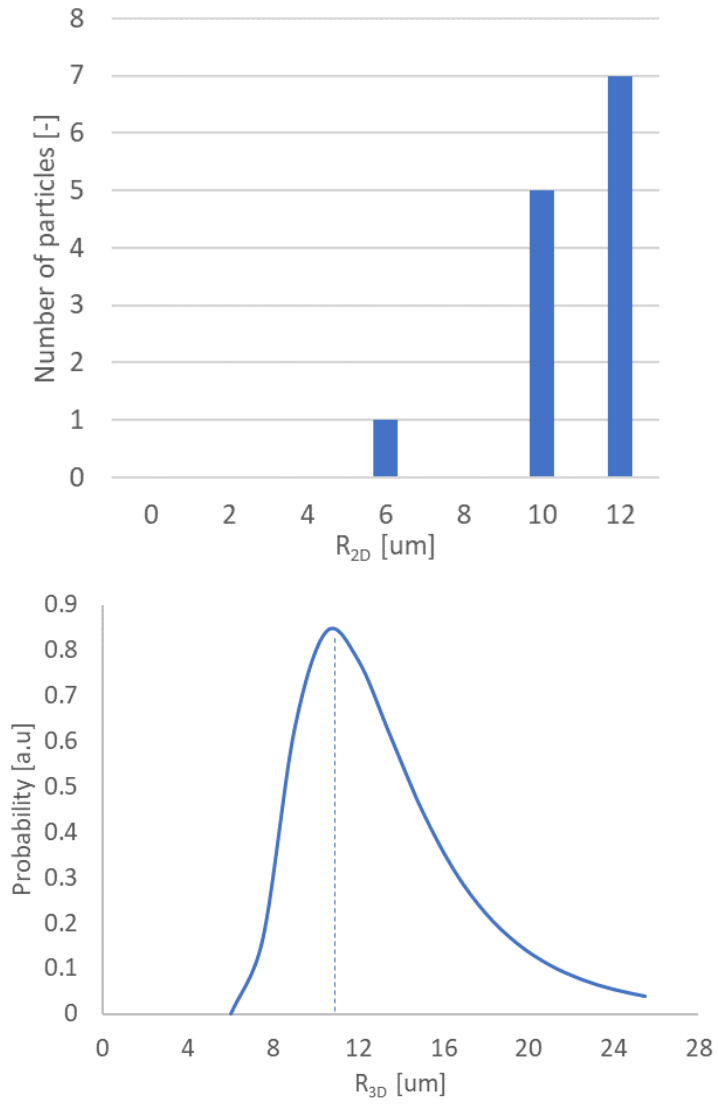


Fig. 3

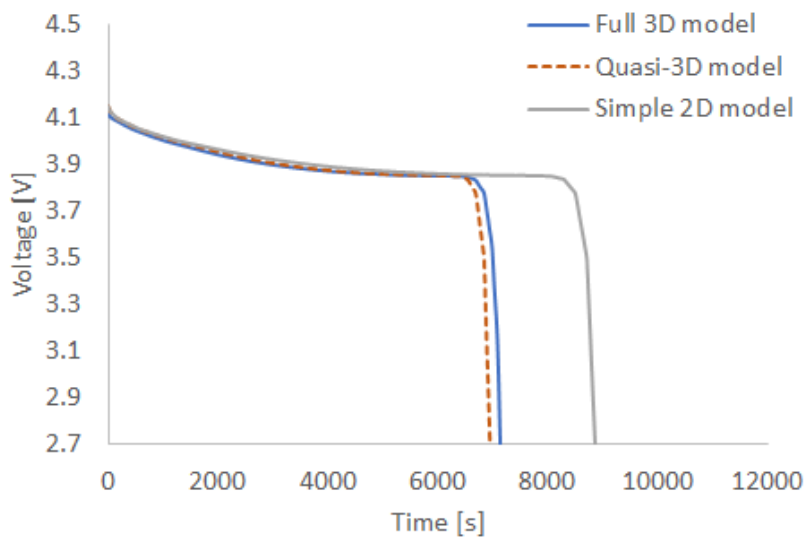


Fig. 4

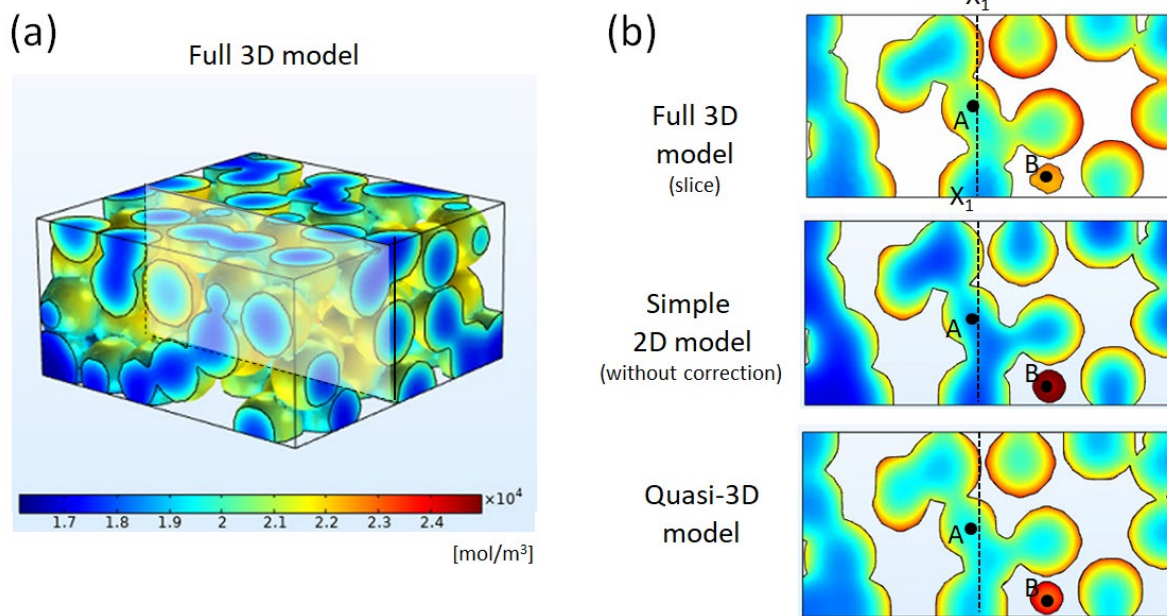
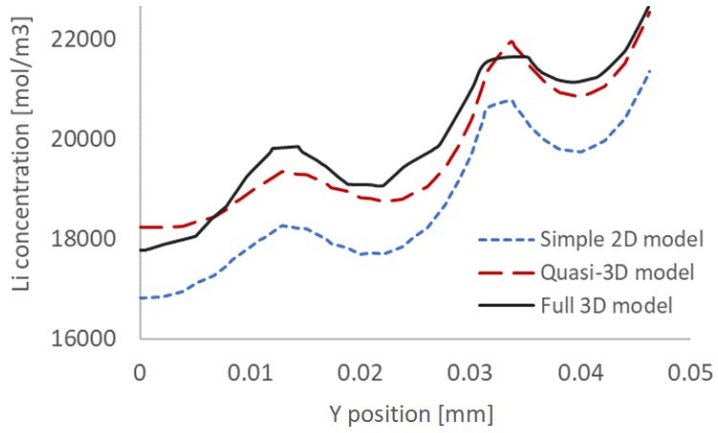
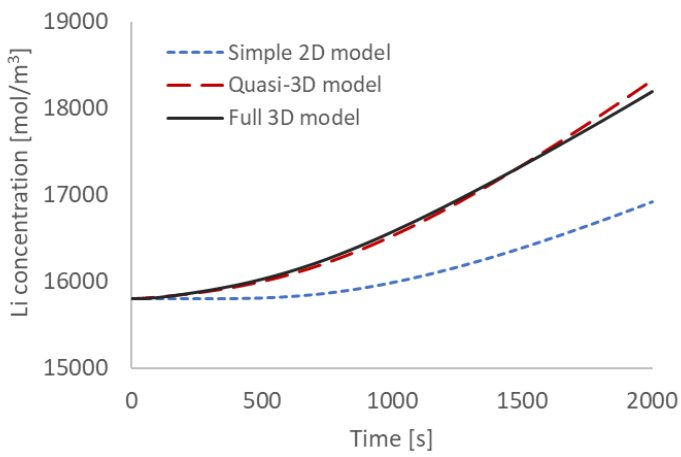


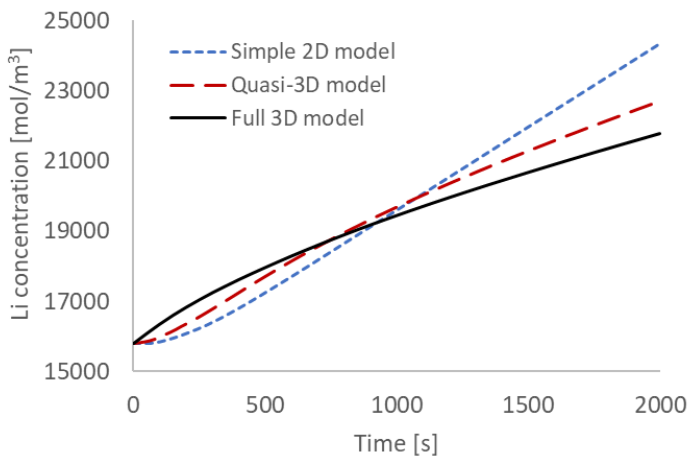
Fig. 5



(a)



(b)



(c)

Fig. 6

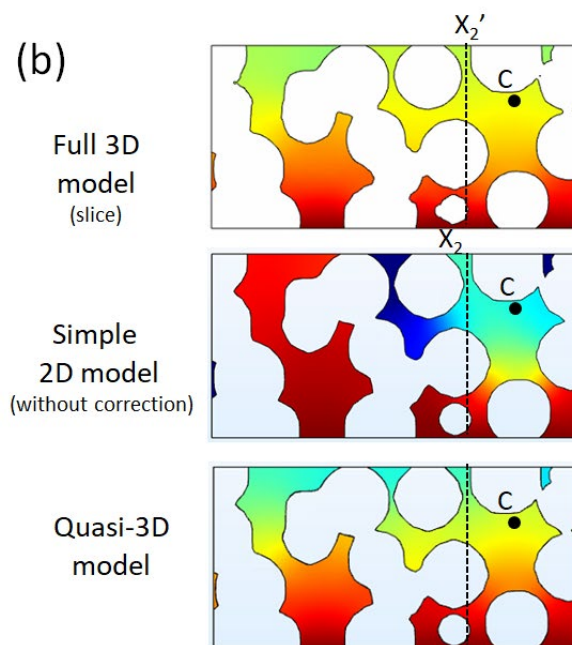
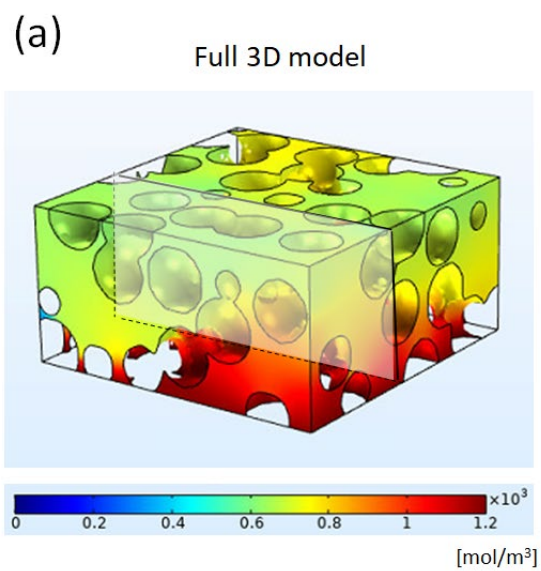
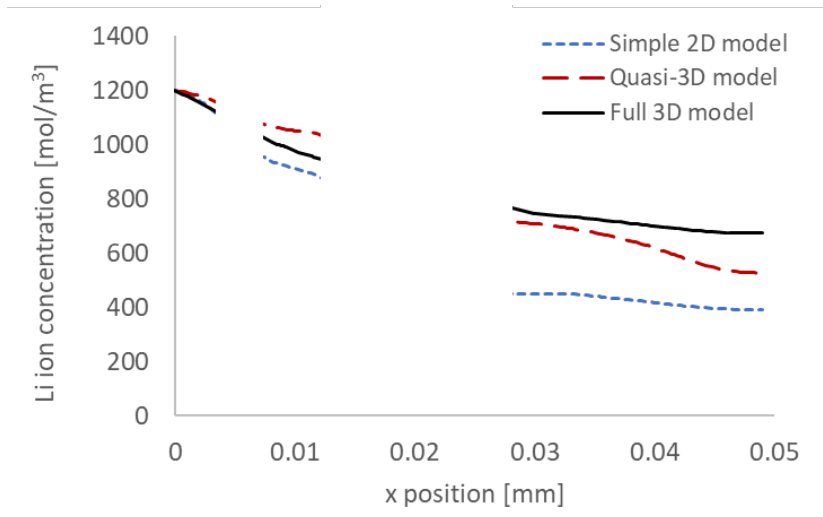
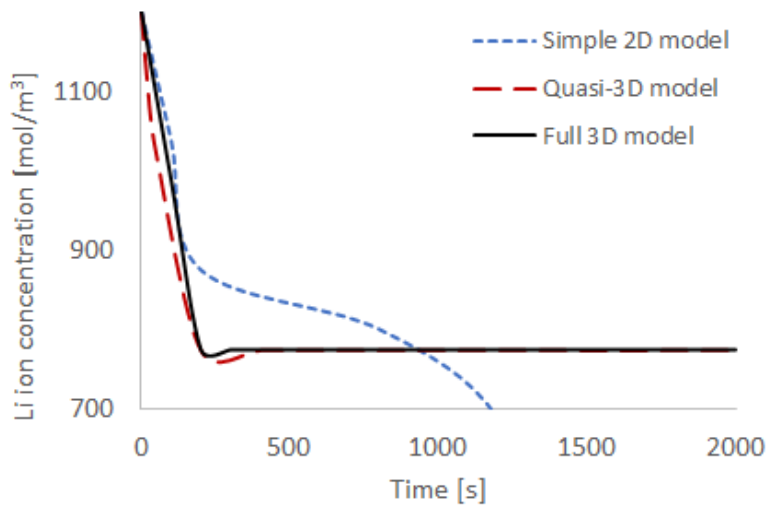


Fig. 7



(a)



(b)

Fig. 8

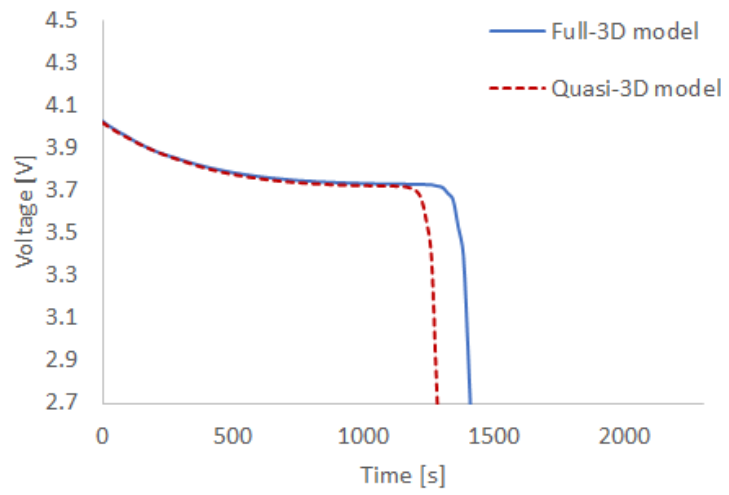
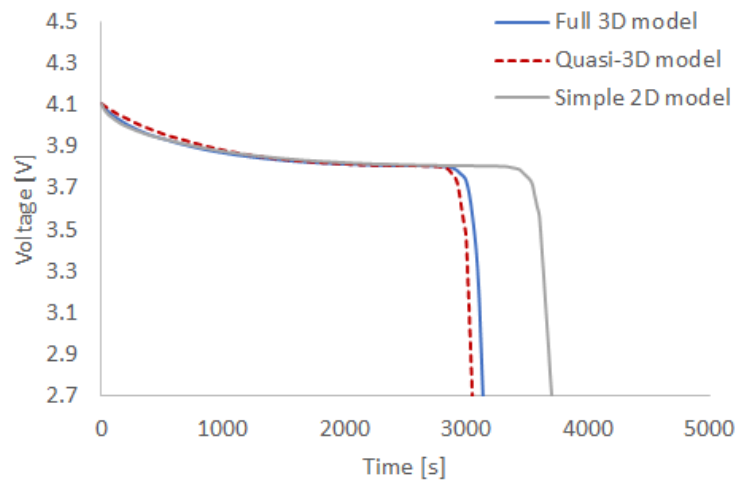


Fig. 9

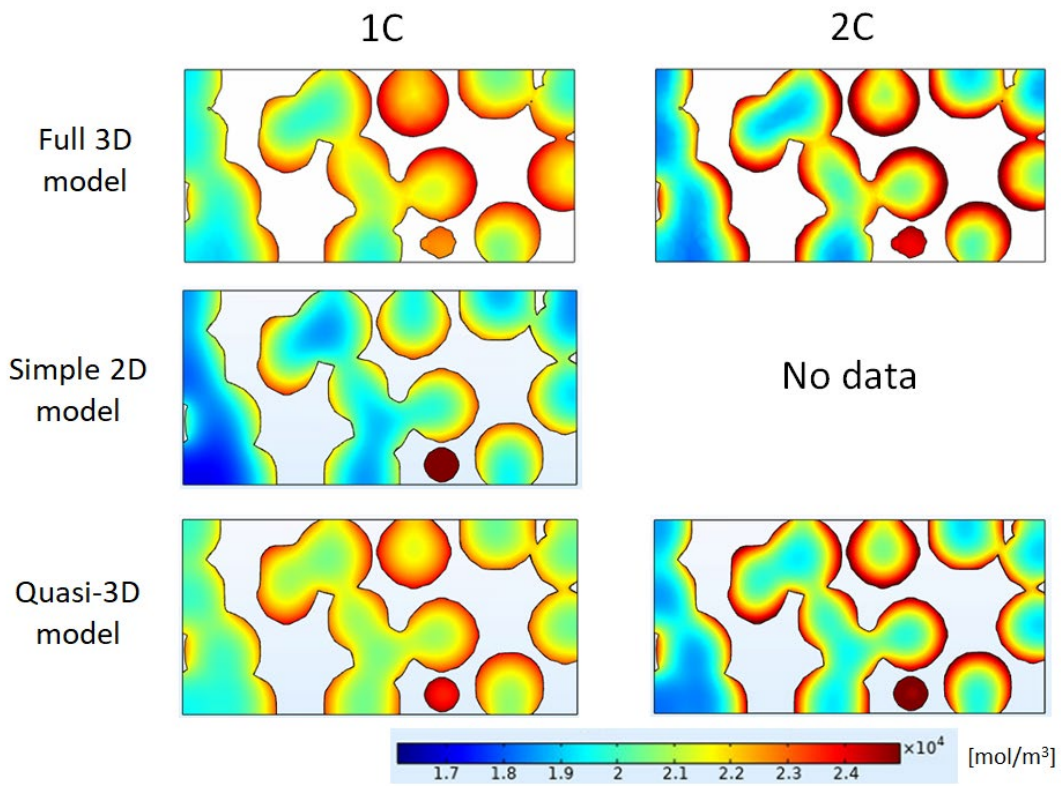


Fig. 10

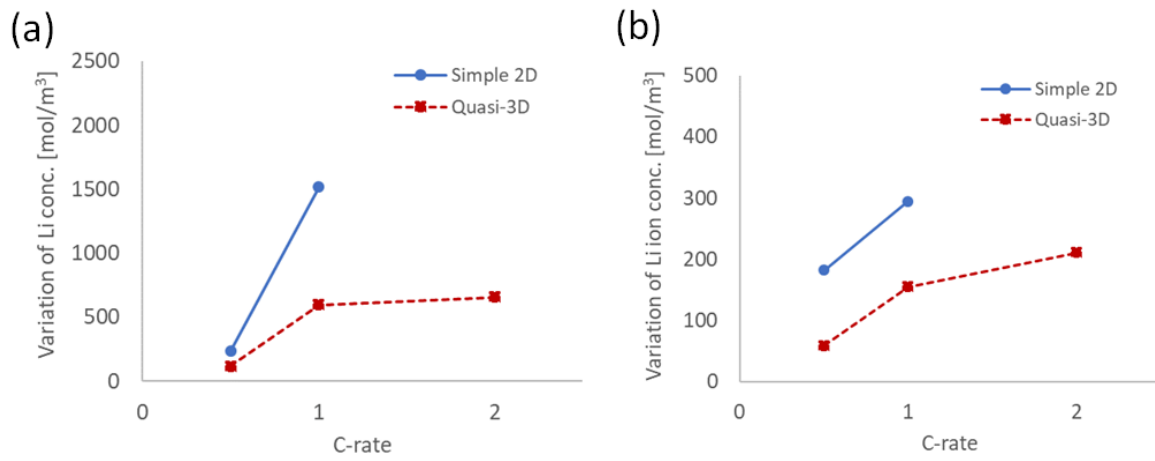
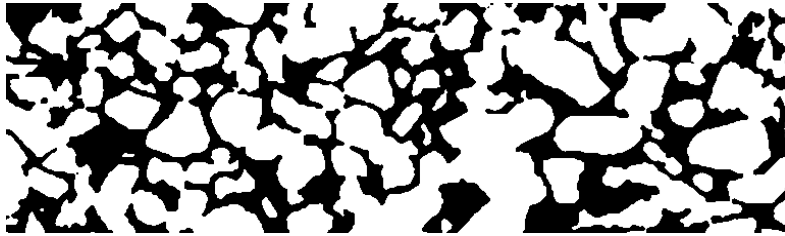


Fig. 11



(a)



(b)

Fig. 12

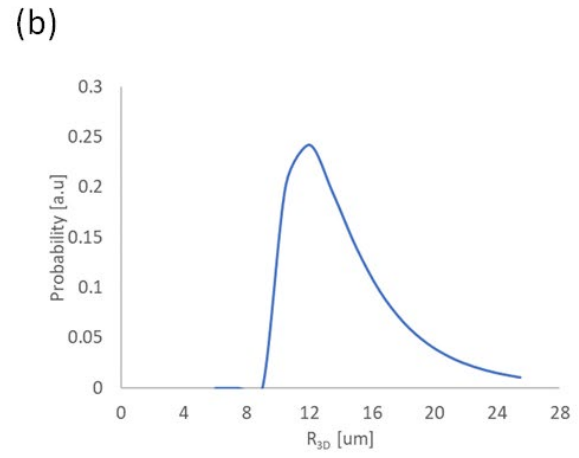
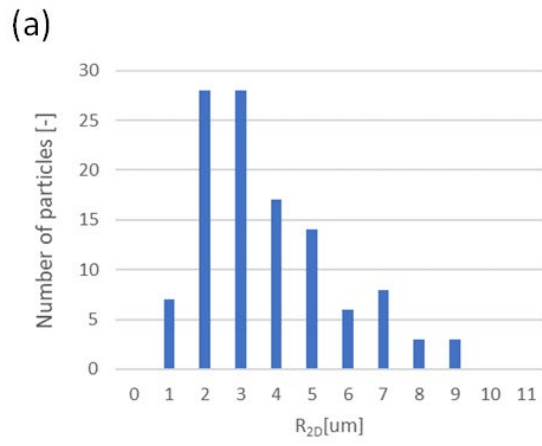


Fig. 13

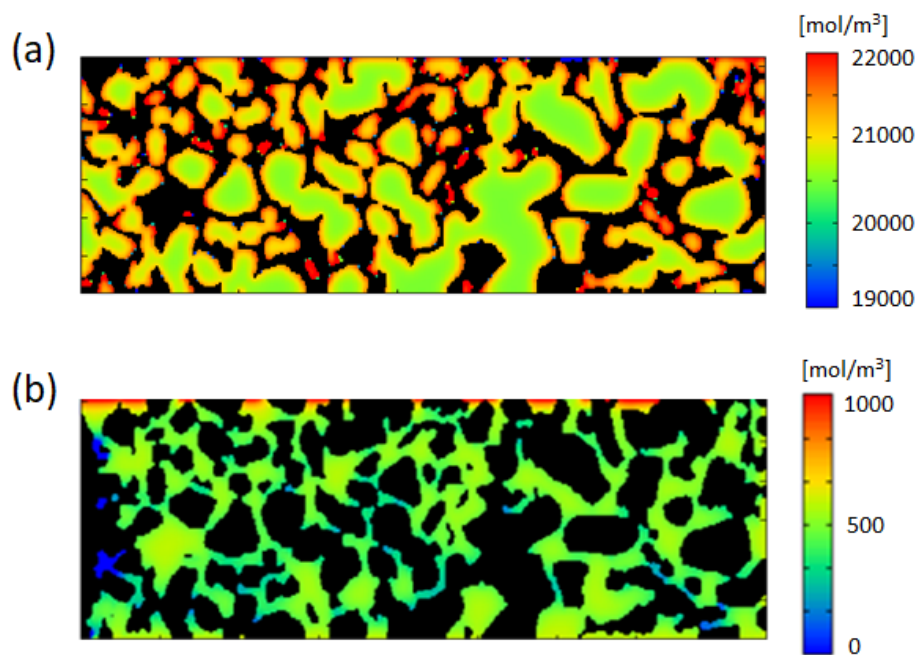


Fig. 14

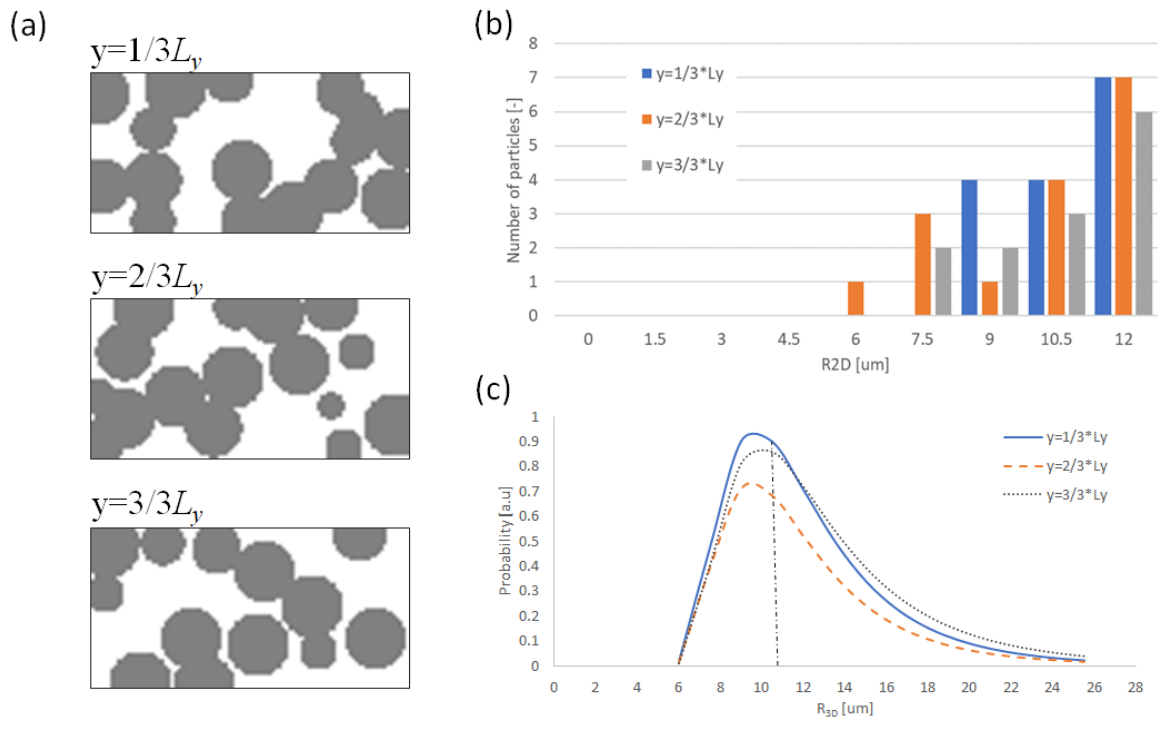


Fig. 15